Hydrothermal preparation and Magnetic Properties of $NaFeSi_2O_6$: Nanowires vs Bulk Samples

Shiliang Zhou,[†] Wolfgang G. Zeier,[†] Moureen Kemei,[‡] Moulay T. Sougrati,[¶] Matthew Mecklenburg,[§] and Brent C. Melot[*,†]

Department of Chemistry, University of Southern California, Los Angeles, CA 90089, Materials Department, University of California, Santa Barbara, CA 93106-5121, Institut Charles Gerhardt-Laboratoire des Agrégats, Interfaces et Matériaux pour l'Energie, CNRS UMR 5253, 34095 Montpellier Cedex 5, France, and Center for Electron Microscopy and Microanalysis, University of Southern California, Los Angeles, CA 90089

E-mail: melot@usc.edu

[*]To whom correspondence should be addressed

[†]Department of Chemistry, University of Southern California, Los Angeles, CA 90089

[‡]Materials Department, University of California, Santa Barbara, CA 93106-5121

[¶]Institut Charles Gerhardt-Laboratoire des Agrégats, Interfaces et Matériaux pour l'Energie, CNRS UMR 5253, 34095 Montpellier Cedex 5, France

[§]Center for Electron Microscopy and Microanalysis, University of Southern California, Los Angeles, CA 90089

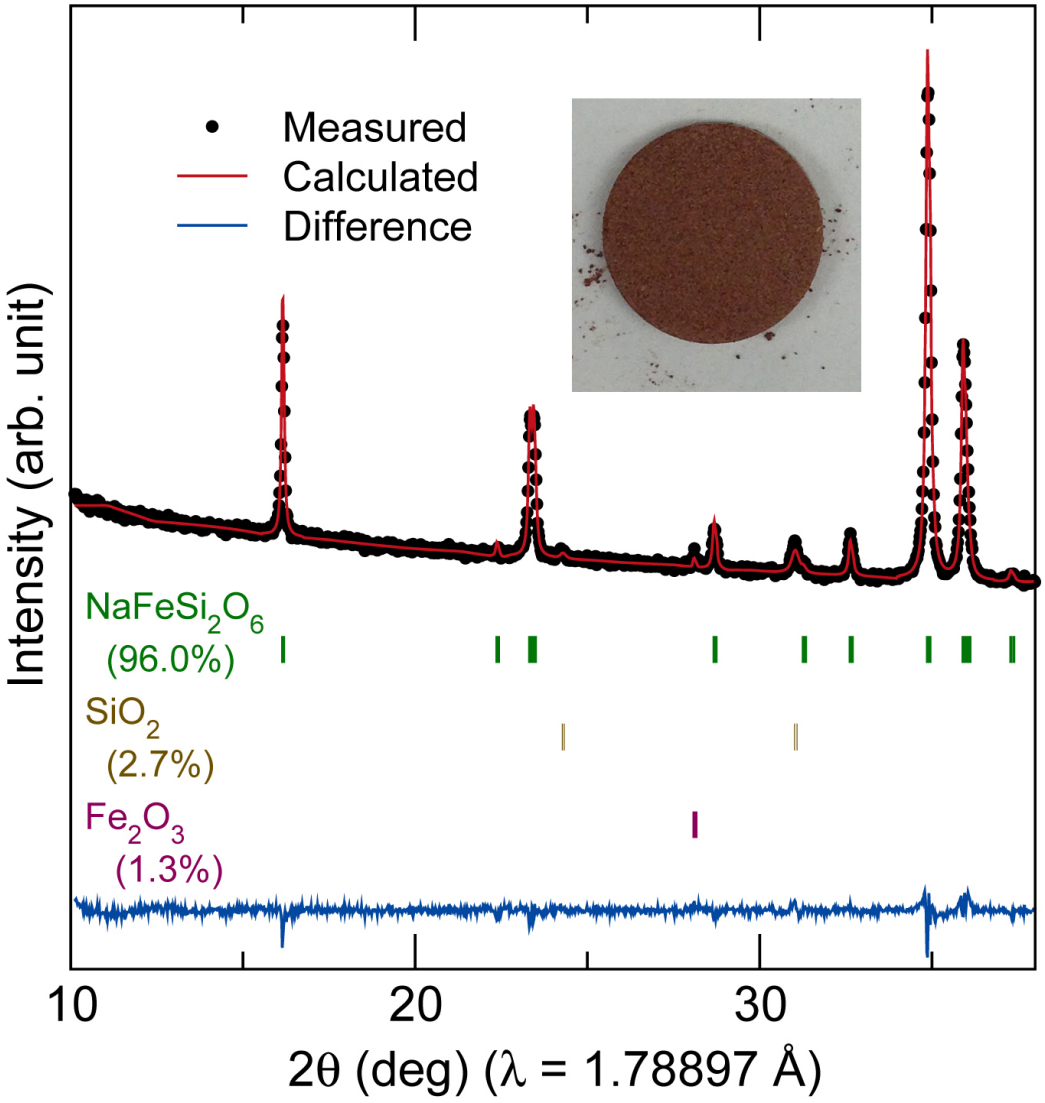

Figure S 1: Rietveld refinement of the impure, red colored $NaFeSi_2O_6$ sample from ceramic reaction at 750°C against laboratory X-ray diffraction data. Small Fe_2O_3 impurities result in a red color (inset), in contrast to the yellowish-green color of the phase pure compound.

Table S 1: Resulting unit cell parameters and reliability factors from the Rietveld refinement of the as-prepared and sintered $NaFeSi_2O_6$ against synchrotron X-ray powder diffraction data.

	As-prepared	Sintered
Space group	C 2/c	C 2/c
a (Å)	9.67696(12)	9.65827(1)
b (Å)	8.80278(11)	8.80896(1)
c (Å)	5.30001(7)	5.28710(1)
β (deg)	107.37506(13)	107.32134(13)
V (Å^3)	430.876(9)	429.423(1)
R_{wp}	11.7	7.24
χ^2	2.42	2.28

Table S 2: Resulting atomic positions and isotropic atomic displacement parameters (ADP) from the Rietveld refinement of the as-prepared (top) and sintered (bottom) $NaFeSi_2O_6$ against synchrotron X-ray powder diffraction data. The ADPs of one or two of the oxygen atoms become negative once they are included in the refinement, which is probably due to the low scattering form factor of oxygen and statistical error. For the consistency and simplicity of the refinement, the ADPs of all oxygen atoms are locked at a reasonable value ($B_{iso} = 0.3$ Å^2).

atom	Wyckoff	x	y	z	B_{iso} (Å^2)
As-prepared $NaFeSi_2O_6$					
Na	4e	0.00000(0)	0.30086(45)	0.25000(0)	1.183(98)
Fe	4e	0.00000(0)	0.89887(20)	0.25000(0)	0.219(30)
Si	8f	0.29015(15)	0.08833(25)	0.23651(33)	0.731(37)
O1	8f	0.11655(30)	0.08193(45)	0.13909(62)	0.300(0)
O2	8f	0.35599(32)	0.26099(41)	0.29577(68)	0.300(0)
O3	8f	0.35956(41)	0.00365(30)	0.01787(106)	0.300(0)
Sintered $NaFeSi_2O_6$					
Na	4e	0.00000(0)	0.30009(12)	0.25000(0)	0.996(26)
Fe	4e	0.00000(0)	0.89834(5)	0.25000(0)	0.430(13)
Si	8f	0.29047(5)	0.08992(7)	0.23428(10)	0.419(14)
O1	8f	0.11416(9)	0.07956(14)	0.13952(19)	0.300(0)
O2	8f	0.35859(10)	0.25580(12)	0.30006(19)	0.300(0)
O3	8f	0.35215(12)	0.00779(10)	0.01177(29)	0.300(0)

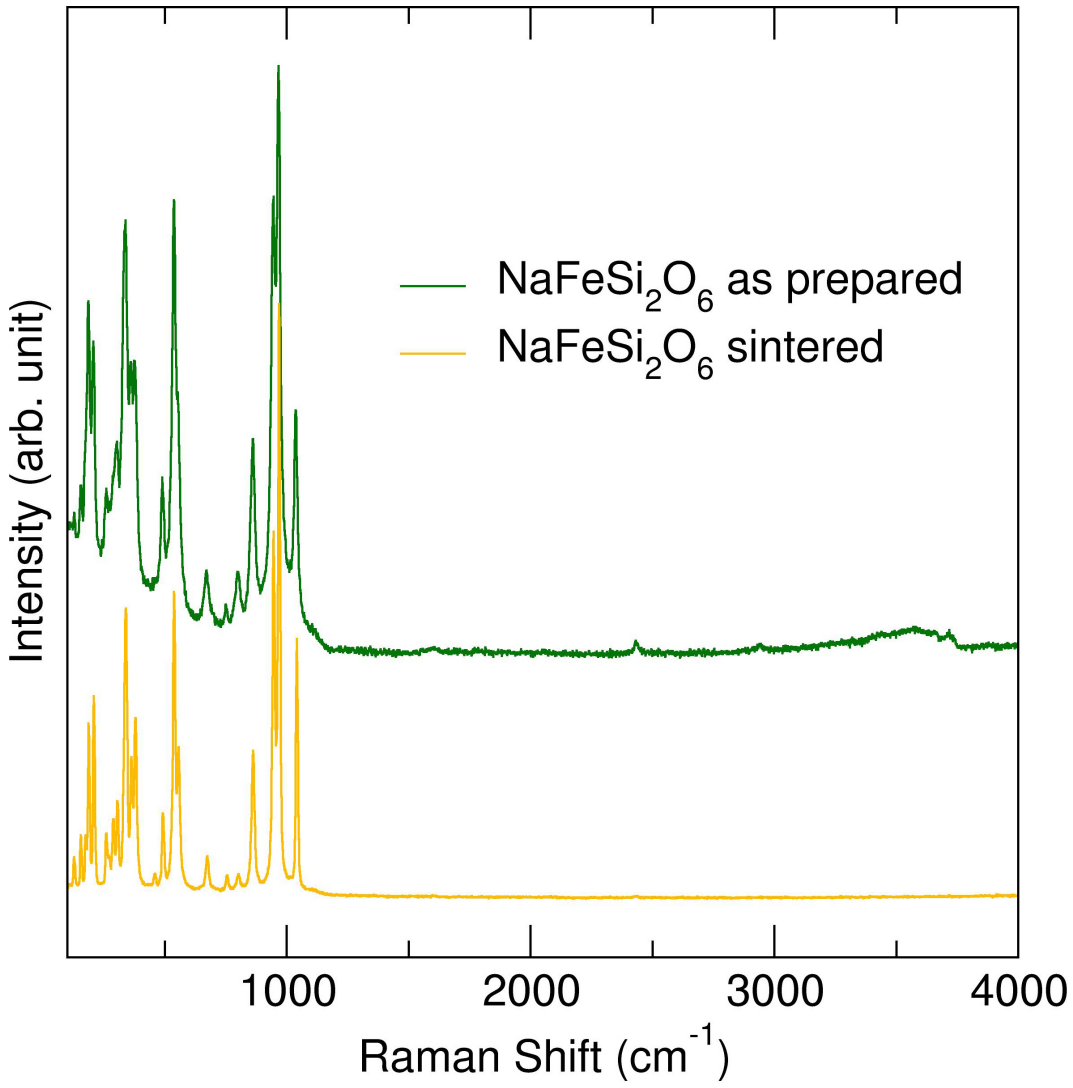

Figure S 2: Raman spectroscopy of the as-prepared and sintered $NaFeSi_2O_6$. The bump centered around $3500\,cm^{-1}$ of the as-prepared samples indicates the presence of surface hydroxyls.

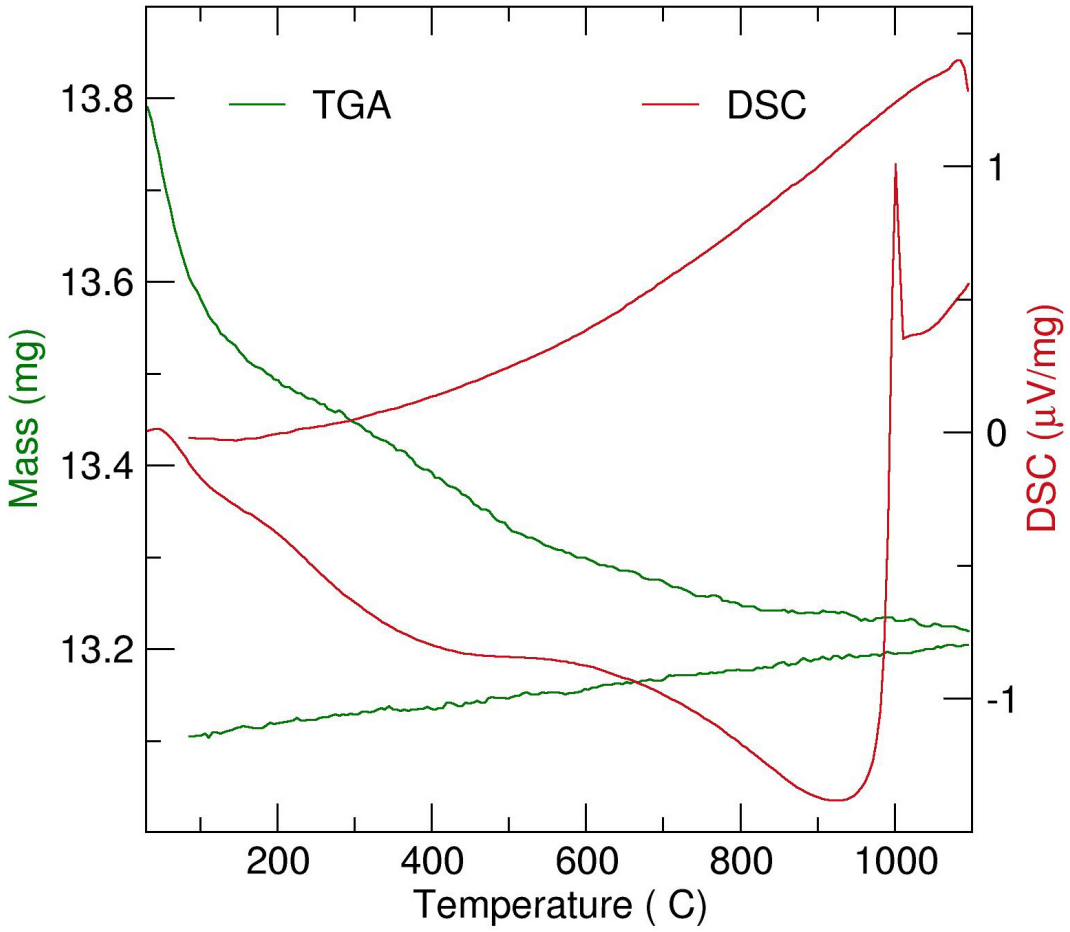

Figure S 3: Simultaneous DSC-TGA analysis of the as-prepared $NaFeSi_2O_6$ nanowires in the temperature range of 30 °C to 1100 °C. The sample was dried at 110 °C prior to the analysis. The melting point of the as-prepared $NaFeSi_2O_6$ was found to be around 1000 °C. A continuous weight loss (4% in total in the heating process) is probably due to the loss of the hydroxyls in the sample.

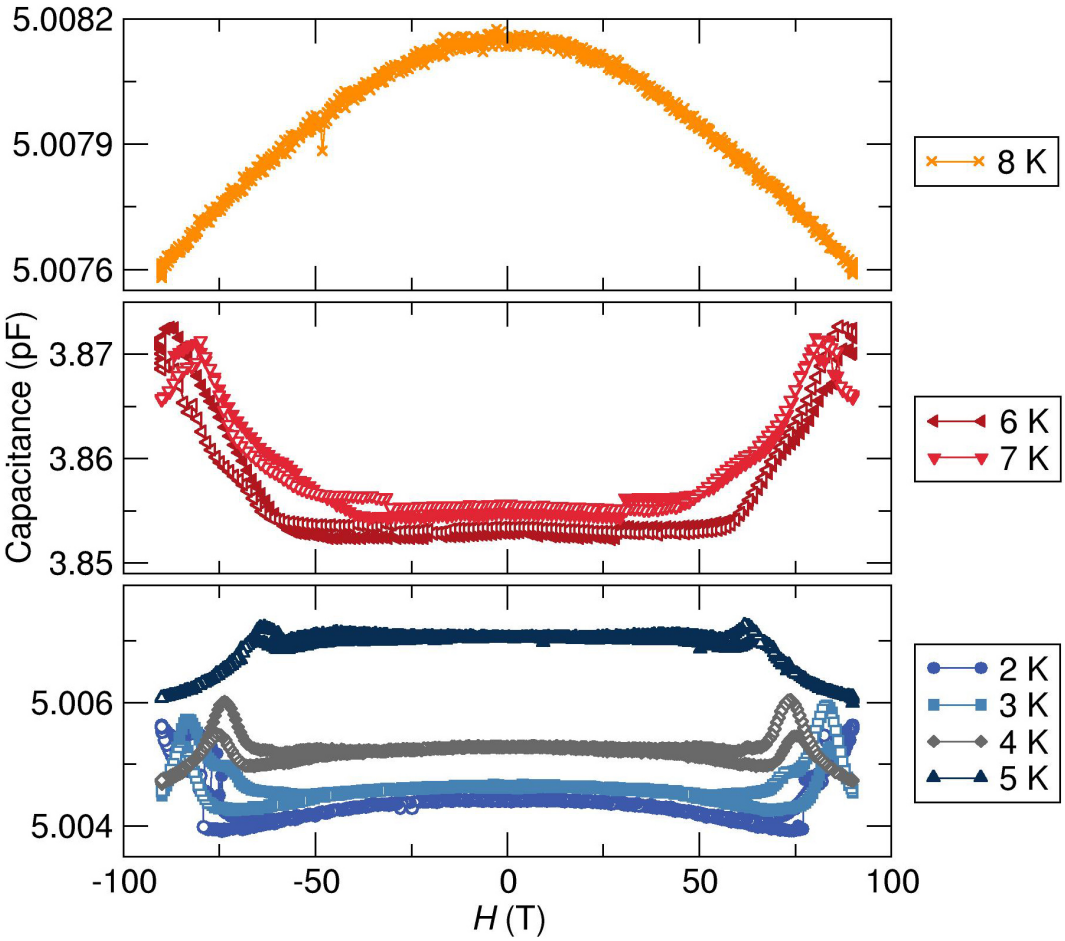

Figure S 4: Field-dependent capacitance measurements of sintered $NaFeSi_2O_6$. There is only fairly weak dependence of the capacitance on the applied field above T=8 K. However, when the temperature is below 7 K, significant enhancement of capacitance when H$\geq$50 kOe and a temperature dependence of this enhancement was observed.

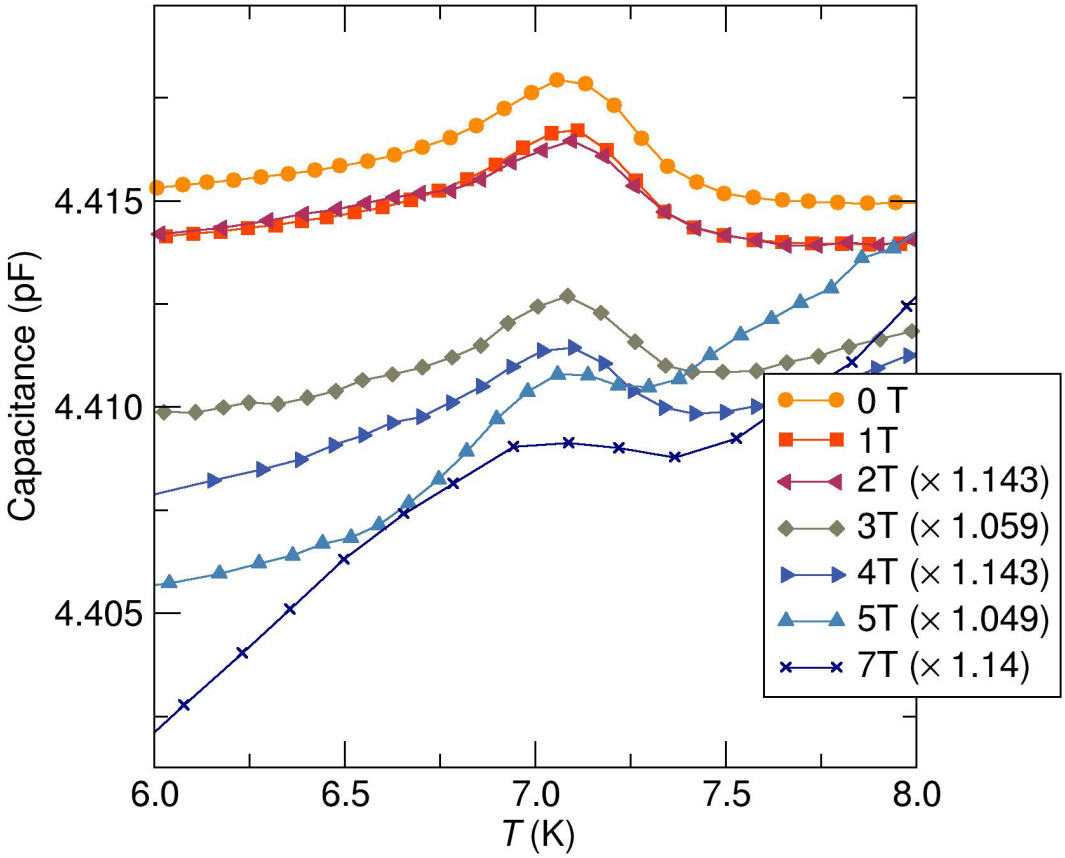

Figure S 5: Temperature dependent capacitance measurements of sintered $NaFeSi_2O_6$. A clear change in the capacitance is observed at T$\simeq$7 K. It is also shown that this change is suppressed by an applied field. The measurement was conducted on warming at 1000 Hz.

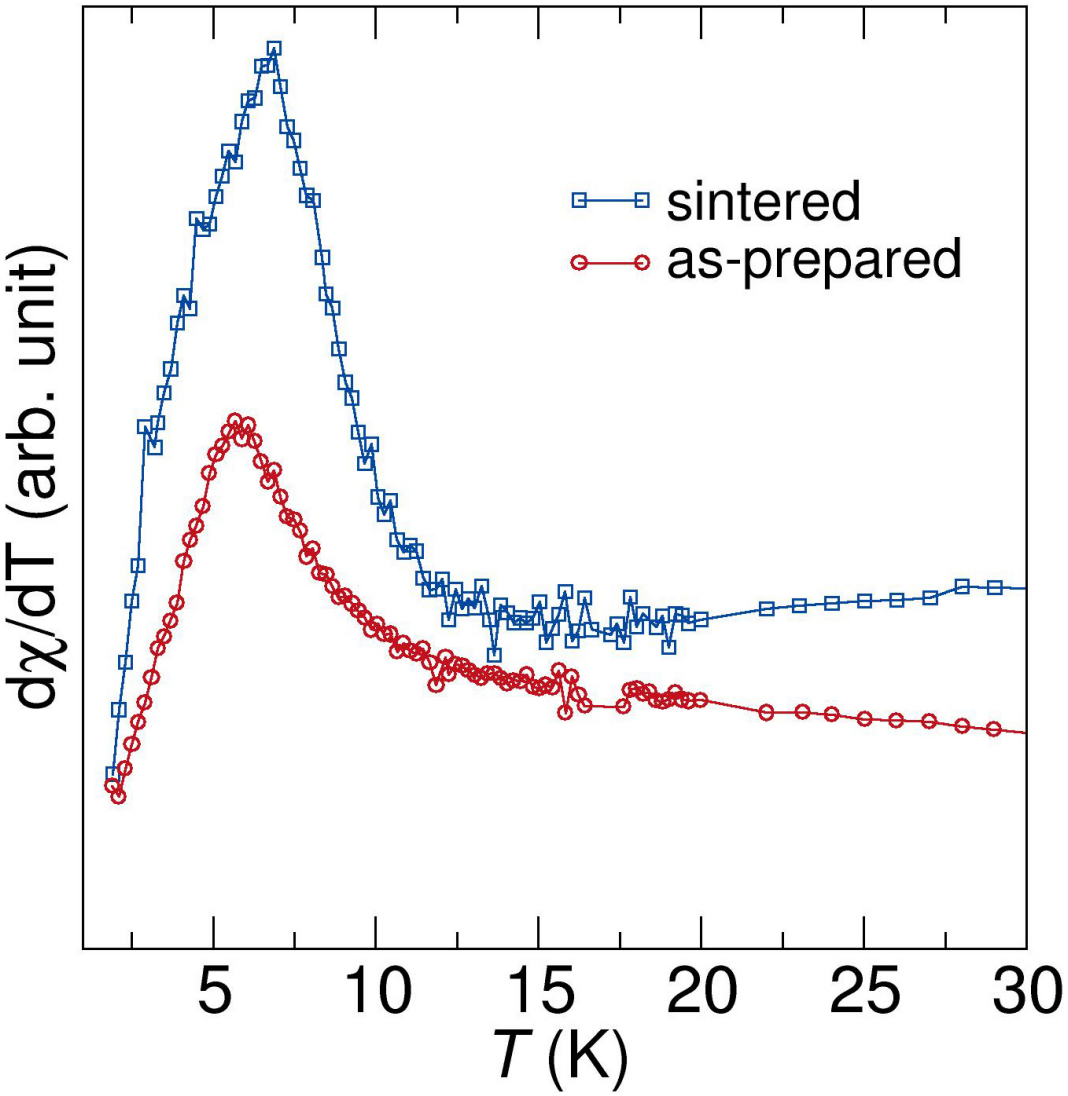

Figure S 6: First derivative curves of the temperature-dependent magnetic susceptibility of the as-prepared $NaFeSi_2O_6$ nanowires and sintered sample. The derivatives show a single maximum at 6 K for the nanowires and 7 K for the sintered material.

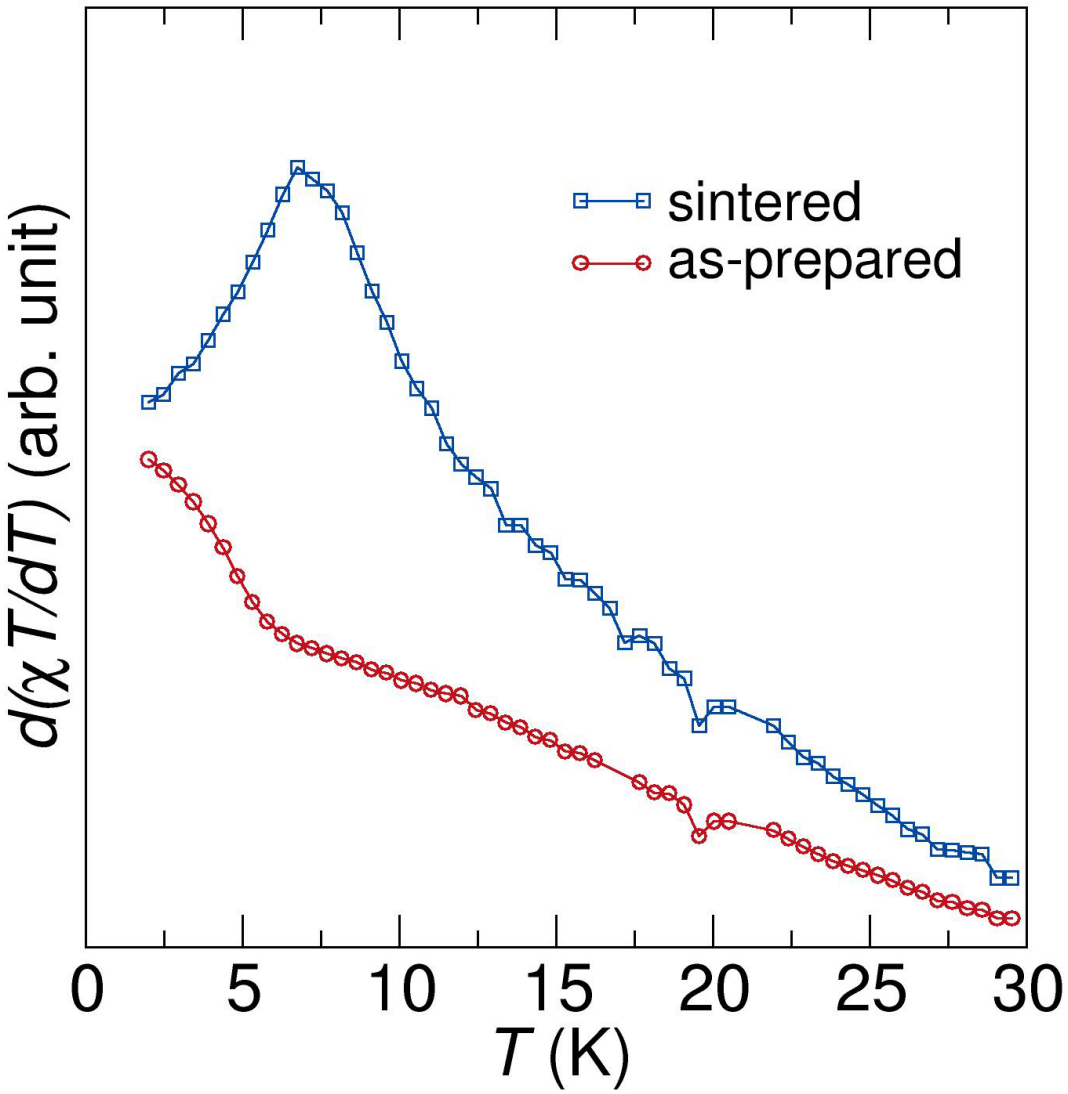

Figure S 7: Fisher heat capacity of $NaFeSi_2O_6$ determined by using magnetic susceptibility data shown in Fig. 6.

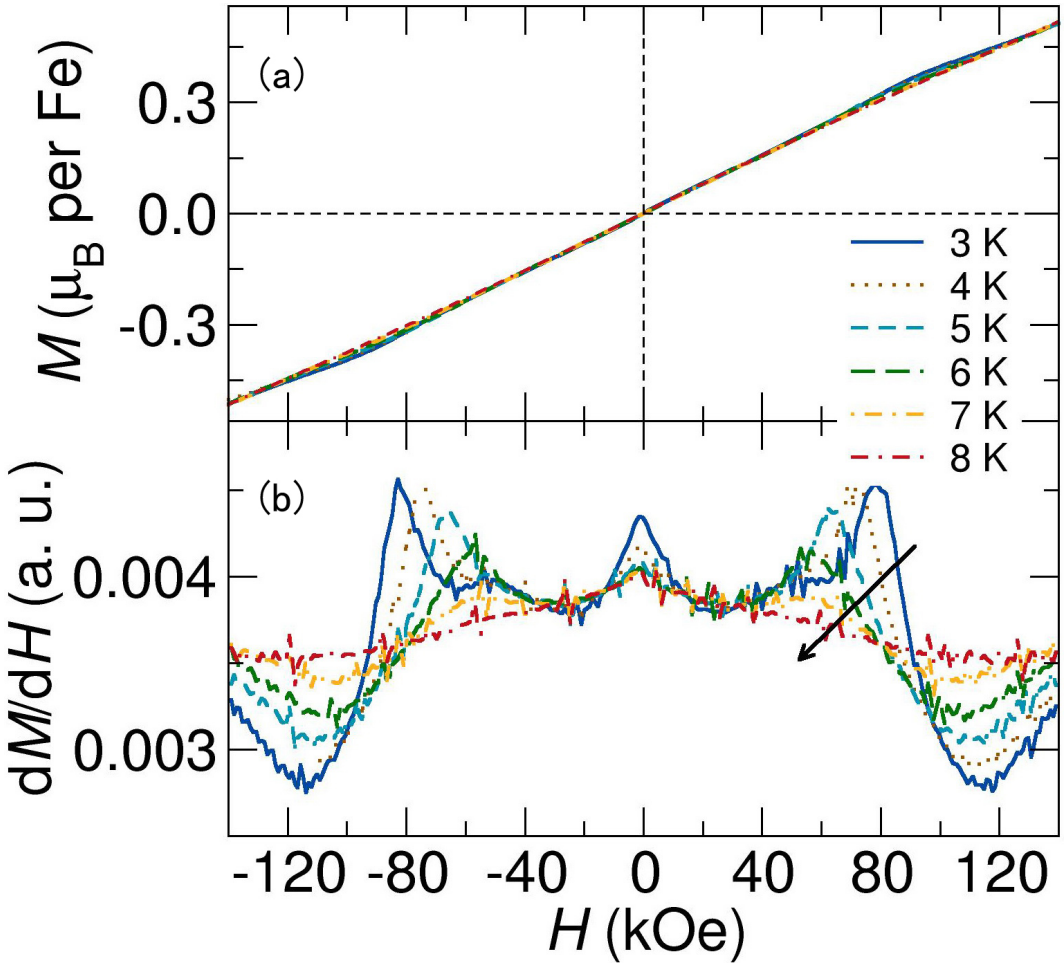

Figure S 8: Constant temperature magnetization loops of sintered $NaFeSi_2O_6$. Two distinct field-induced features are observed at 3 K and 2 K [Fig. 8(a)]. Only the feature at higher field persists at temperatures above 3 K.